Vector mesons and DVCS

L. Adamczyk[a] (on behalf of the H1 and ZEUS collaborations)

[a]University of Science and Technology, Department of Physics and Applied Computer Science, Al. Mickiewicza 30, 30-059 Cracow, Poland

Recent experimental results on diffractive vector meson (VM) production and deeply virtual Compton scattering (DVCS) from the H1 and ZEUS collaborations are reviewed. The data are compared with theoretical predictions.

1. Introduction

High-energy diffractive vector meson production and deeply virtual Compton scattering are experimentally clean processes which allow investigation of the nature of the strong interaction. HERA provides simultaneous control of several scales: the mass of the vector meson M_{VM}, the virtuality of the exchanged photon, Q^2, and the four-momentum transferred at the proton vertex, t. The studies at HERA allow the transitions from *soft* to *hard* regime as a function of the various scales to be investigated.

In figure 1 the cross section for elastic vector meson photoproduction ($Q^2 \approx 0$) is shown as a function of the photon-proton center-of-mass energy W. Light vector meson production with small momentum transfers displays features characteristic of soft diffractive processes, and are well described within the framework of the vector meson dominance model and Regge phenomenology. At high energy, in Regge theory, the cross section is dominated by the "soft Pomeron" trajectory(represented by a soft Pomeron exchange diagram in Fig.2). Its intercept describes the observed weak energy dependence $\propto W^{0.2}$ of the elastic light vector meson photoproduction cross section. When the vector meson mass is large, the cross section increases with energy faster than expected for soft processes. This behaviour can be explained in the framework of perturbative QCD (pQCD) models[1], in which the process is described by the exchange of two gluons or a gluon ladder, and the hard scale is given by large Q^2 or large mass of the final-state meson(represented by a two-gluon exchange diagram in Fig.2). The fast rise of the cross sections with W ($\sigma \propto W^{0.8}$) is due to the rise of the gluon density in the proton at low x.

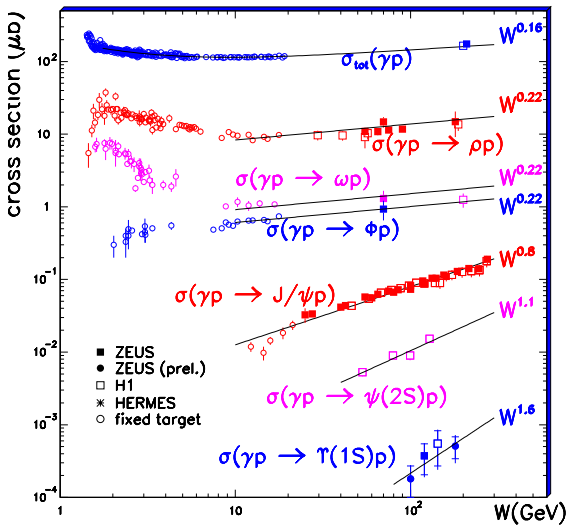

Figure 1. Cross sections as a function of W of the elastic photoproduction of $\rho, \omega, \phi, J/\Psi, \Psi'$ and Υ vector mesons. The solid lines represent fits of the W^δ dependence.

In the vector meson dominance model, the vector meson retains the helicity of the photon, therefore, s-channel helicity conservation (SCHC)

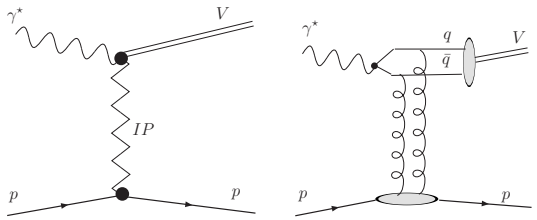

Figure 2. Diagrams describing elastic vector meson production in terms of the Pomeron (left diagram) and two-gluon exchange (right diagram).

is satisfied. In the region dominated by perturbative QCD breaking of SCHC is expected[2].

The DVCS process is similar to diffractive vector meson production, replacing the final state vector meson by a real photon. In QCD calculations [3,4], DVCS avoids uncertainties associated with unknown wave function of the produced vector meson. The calculations assume that the DVCS reaction involves two partons in the proton which carry different longitudinal and transverse momenta. This difference, also called skewing, is a consequence of the mass difference between the incoming virtual photon and the produced real photon. The skewing can be described using generalised parton distributions(GPD) [5].

2. W dependence in electroproduction

The transition from *soft* to *hard* regime can be investigated by varying Q^2 for a given vector meson. Figure 3 shows the cross section for elastic electroproduction of ρ^0 mesons measured by ZEUS[6], as a function of W, for different values of Q^2. The W dependence is found to become steeper with increasing Q^2 and tends toward the same value as for J/Ψ photoproduction. The W dependence is characterised by power law fits of the form $\sigma \propto W^\delta$ represented by the lines in Figure 3.

The W^δ parametrisation is inspired by the Regge description of soft interaction. Assuming a linear form $\alpha(t) = \alpha(0) + \alpha' t$ of the Regge trajectory, δ can be translated into the intercept $\alpha(0)$

$$\alpha(0) = 1 + \delta/4 - \alpha' \langle t \rangle \,.$$

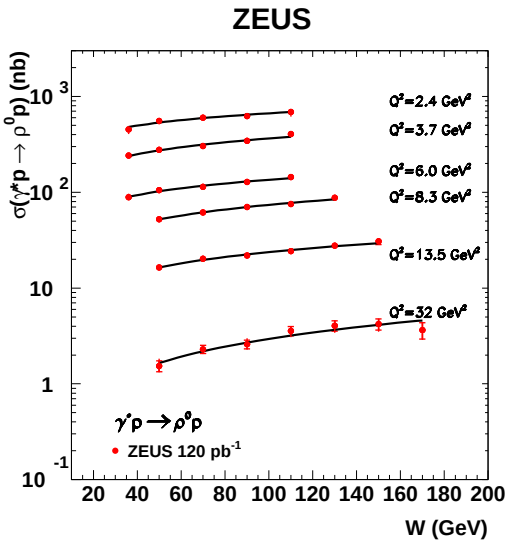

Figure 3. The W dependence of the cross section for elastic electroproduction of ρ^0 mesons for various Q^2 values as indicated in the figure. The solid lines are the results of a fit of the form W^δ to the data.

Figure 4 shows the values of $\alpha(0)$ obtained for electroproduction of ρ^0 [6–8] as well as those for ϕ [7,9], J/Ψ [10,11] and DVCS [12]. The results are plotted as a function of $Q^2 + M^2_{VM}$. One observes a universal behaviour, showing an increase of $\alpha(0)$ as the scale becomes larger, in agreement with the expectations mentioned in the introduction. The value of $\alpha(0)$ at low scale is in agreement with the value expected from the soft Pomeron intercept shown as the dashed line in Figure 4.

3. t dependence of the cross section

The differential cross section, $d\sigma/dt$, has been parametrised by an exponential function e^{bt}. The slope b determines the area size of the interaction region, which depends on the proton radius

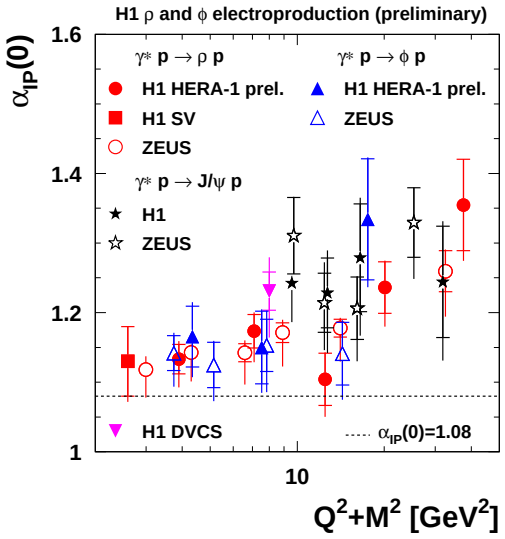

Figure 4. A compilation of the values of $\alpha(0)$ for exclusive electroproduction of vector mesons as a function of $Q^2 + M^2_{VM}$. It includes also the DVCS results. The value 1.08, typical for soft diffraction, is indicated by the dashed line.

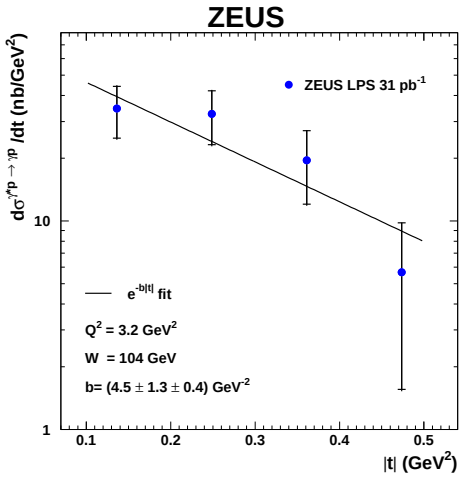

Figure 5. The differential cross section $d\sigma/dt$ for DVCS. The line is the best fit of an exponential form to the data, yielding the slope b quoted in the figure.

and on the size of the produced vector meson or real photon. For exclusive diffractive processes at large values of $(Q^2 + M^2_{VM})$ the typical size of the vector meson or real photon is small, and the slope b is determined entirely by the proton radius.

The first direct measurement of the DVCS differential cross section as a function of t, extracted from the ZEUS Leading Proton Spectrometer tagged events [13], is shown in Figure 5 for $Q^2 = 3.2\,\mathrm{GeV}^2$. The value of the slope extracted from a fit is $b = 4.5 \pm 1.3(\mathrm{stat.}) \pm 0.4(\mathrm{syst.})\ \mathrm{GeV}^{-2}$. This value is consistent with the result obtained by H1 [14] $b = 5.45 \pm 0.19(\mathrm{stat.}) \pm 0.34(\mathrm{syst.})\ \mathrm{GeV}^{-2}$ at $Q^2 = 8\ \mathrm{GeV}^2$, from the transverse momentum distribution of the produced photon.

Figure 6 shows the values of the slope b obtained for electroproduction of ρ^0 [6,8,15] as well as those for ϕ [9], J/Ψ [10,11] and DVCS [12–14]. The results are plotted as a function of

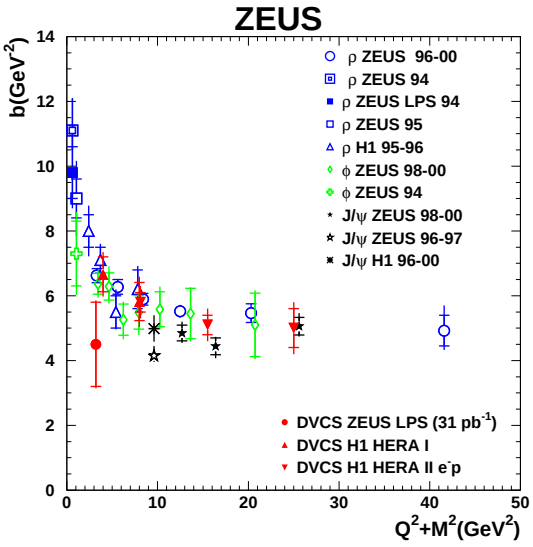

Figure 6. A compilation of the values of the slope b for exclusive electroproduction of vector mesons as a function of $Q^2 + M^2_{VM}$. It includes also the DVCS results.

$Q^2 + M_{VM}^2$. As expected, b decreases to a universal value about 5 GeV^{-2} as the scale increases. Assuming that the process of exclusive electroproduction of vector mesons or DVCS are dominated by gluons, the value of $b = 5\ GeV^{-2}$ corresponds to the radius of the gluon density in the proton of about 0.6 fm. This value is smaller than the value 0.8 fm of charge density of the proton, indicating that gluons are well contained within the charge-radius of the proton.

4. Generalised parton distribution

As was mentioned in the introduction, QCD calculations of the DVCS reaction necessitates the use of GPD. The analysis of the DVCS process can be used to investigate the GPD formalism. The DVCS cross section integrated over t can be written [3] as

$$\sigma_{DVCS} = \frac{[\mathcal{I}mA(\gamma^\star p \to \gamma p)]^2(1+\eta^2)}{16\pi b},$$

where $\mathcal{I}mA(\gamma^\star p \to \gamma p)$ is the imaginary part of the $\gamma^\star p \to \gamma p$ amplitude at $t = 0$ and η^2 is a small correction due to the real part of the amplitude. The amplitude $A(\gamma^\star p \to \gamma p)$ is proportional to the GPD. The Q^2 evolution of the GPD is accessed from the data by removing other Q^2 dependences from the measured cross section. For this purpose, the dimensionless observable S is defined [16] as

$$S = \sqrt{\frac{\sigma_{DVCS} Q^4 b}{(1+\eta^2)}}.$$

Figure 7 shows the observable S as a function of Q^2 obtained from measurements by H1 [12,14] together with the prediction of a GPD model [16]. It is found that the GPD model reproduces well both the DVCS amplitude and its weak rise with Q^2.

The magnitude of the skewing effects present in the DVCS process can be extracted by constructing the ratio of the imaginary parts of the DVCS and DIS amplitudes. In leading order, this ratio $R = \mathcal{I}mA(\gamma^\star p \to \gamma p)/\mathcal{I}mA(\gamma^\star p \to \gamma p)$ is equal to the ratio of the GPDs to the standard parton distribution functions. Assuming that the

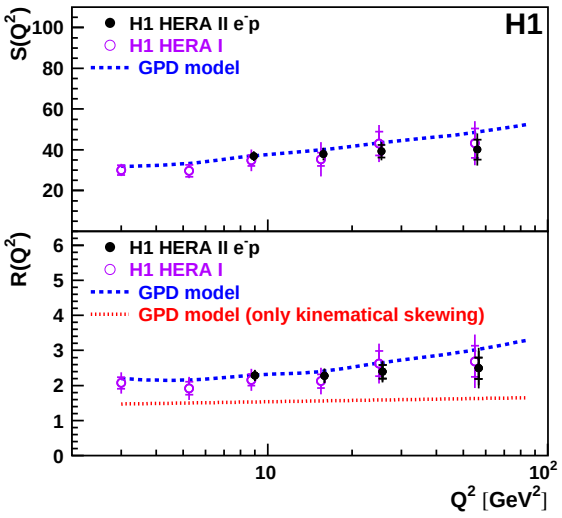

Figure 7. The observables S and R as a function of Q^2. The dashed curves show the predictions of the GPD models. The dotted curve shows the prediction of a GPD model based on an approximation where only the kinematical part of the skewing is taken into account.

virtual photon is mainly transversely polarised in the case of DVCS process, the expression for R can be written as

$$R = \frac{\sqrt{16\pi} S Q^2}{\sigma_T(\gamma^\star \to X)}.$$

The measured values of the ratio R as a function of Q^2 are shown in the bottom plot in figure 7 and are compared with prediction based on the GPD model [16]. The typical values of R are around 2, while in a model without skewing R would be equal to unity. This result confirms the large effect of skewing. In GPD models, two different effects contribute to skewing: the kinematics of the DVCS process and the Q^2 evolution of the GPDs. The result of the model based on an approximation where only the kinematical part of the skewing is taken into account is also presented on Figure 7. Such an approximation is not sufficient to reproduce the total skewing effects observed in the data.

5. Geometric scaling

At very small values of the Bjorken scaling variable x the saturation regime of QCD can be reached. In this domain, the gluon density in the proton is so large that non-linear effects tame its growth. In the dipole model approach, the transition to the saturation regime is characterised by the saturation scale parametrised as $Q_s^2 = Q_0^2(x_o/x)^{-\lambda}$, where Q_0, x_0 and λ are parameters [17]. An important feature of dipole models with saturation is that the total cross section can be expressed as a function of the single variable τ:

$$\sigma_{tot}^{\gamma^\star p}(x,Q^2) = \sigma_{tot}^{\gamma^\star p}(\tau) \quad \text{with} \quad \tau = \frac{Q^2}{Q_s^2(x)}\,.$$

This property, called geometric scaling, has already been observed to hold for the total ep DIS cross section [18,19] as well as in DIS on nuclear targets [20] and in diffractive processes [21].

Figure 8 shows the DVCS cross sections measurements [12,14] taken at different Q^2 and $x = Q^2/W^2$ values as a function of the single variable τ. All of the cross section measurements appear to be well aligned on a single curve. Therefore, the DVCS data are compatible with the geometric scaling law. The dipole model [21,17] provides a good description of the measurements over the complete range of τ.

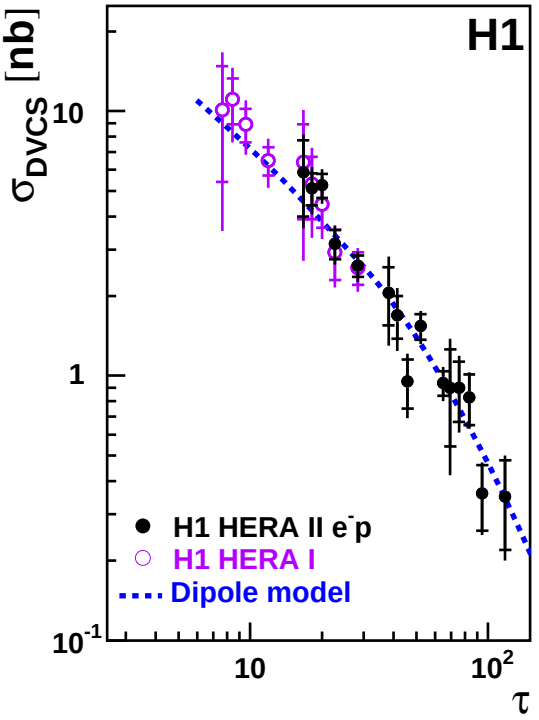

Figure 8. DVCS cross section as a function of the scaling variable $\tau = Q^2/Q_s^2(x)$. The dashed curves represent predictions of the dipole model [21,17].

6. Beam charge asymmetry

At HERA the DVCS process is accessed through the reaction $ep \to e\gamma p$. This reaction also receives a contribution from the purely electromagnetic Bethe-Heitler (BH) process, where the photon is emitted from the electron. In addition, an interference term contributes to the cross section due to the identical final states of both the DVCS and BH processes. The main contribution resulting from the interference is proportional to the cosine of the azimuthal angle ϕ of the photon [22,23]. This angle is defined in the proton rest frame as the angle between the electron scattering plane and the plane defined by the initial virtual photon and the scattered proton. The cross section integrated over ϕ is not sensitive to the interference term, but the interference term can be singled out by the measurement of the cross section asymmetry with respect to the lepton beam charge. For this purpose, differential cross sections for the DVCS process are measured as a function of the azimuthal angle ϕ, separately in e^+p and e^-p data samples. The beam charge asymmetry(BCA) is then derived by building the asymmetry

$$BCA = \frac{d\sigma^+/d\phi - d\sigma^-/d\phi}{d\sigma^+/d\phi + d\sigma^-/d\phi}\,,$$

where σ^+ and σ^- correspond to cross sections measured in e^+p and e^-p, respectively. The BCA measurement by H1 [24] as a function of ϕ is presented in figure 9. The result of the fit of a function $P\cos\phi$ to the data is also displayed. The am-

plitude of the $\cos\phi$ term was found significantly different from zero, $0.17\pm0.03(\text{stat.})\pm0.05(\text{syst.})$. The beam charge asymmetry was obtained for the first time in a colliding mode.

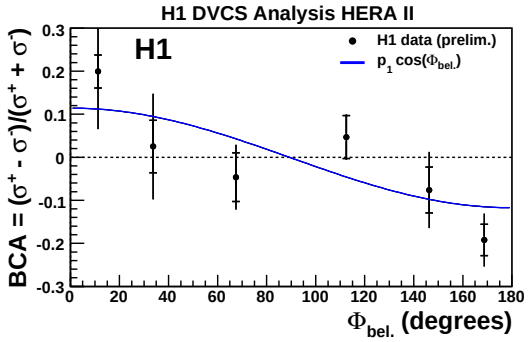

Figure 9. Beam charge asymmetry as a function of ϕ. The line represents the result of a $P\cos\phi$ fit to the data.

REFERENCES

1. See e.g.
   M.G. Ryskin, Zeit. Phys. C **57** (1993) 89;
   S.J. Brodsky *et al.*, Phys. Rev. D **50** (1994) 3134.
2. D.Yu. Ivanov and R. Kirschner, Phys. Rev. D **58** (1998) 114026;
   E. Kuraev, N. Nikolaev and B. Zakharov, JETP Lett. **68** (1998) 696;
   I. Royon and J. Cudell, Nucl. Phys. B **545** (1999) 505;
   I. Royon Phys. Lett., B **513** (2001) 337.
3. L.L. Frankfurt, A. Freund and M. Strikman, Phys. Rev. D **58** (1998) 114001 and *erratum* Phys. Rev. D **59** (1999) 119901E.
4. A. Donnachie and H.G. Dosch, Phys. Lett. B **502** (2001) 74.
5. D. Müller, D. Robaschik, B. Geyer, F.M. Dittes and J. Hořejši, Fortsch. Phys. **42** (1994) 101;
   X. Ji, Phys. Rev. Lett. **78** (1997) 610;
   A.V. Radyushkin, Phys. Rev. D **56** (1997) 5524.
6. S. Chekanov *et al.* [ZEUS Collaboration], PMC Physics A **1** (2007) 6.
7. H1 Collaboration, H1prelim-08-013, `http://www-h1.desy.de/h1/www/publications`.
8. C. Adloff *et al.* [H1 Collaboration], Eur. Phys. J. C **13** (2000) 371;
9. S. Chekanov *et al.* [ZEUS Collaboration], Nucl. Phys. B **718** (2005) 3.
10. A. Aktas *et al.* [H1 Collaboration], Eur. Phys. J. C **46** (2006) 585;
11. S. Chekanov *et al.* [ZEUS Collaboration], Eur. Phys. J. C **24** (2002) 345; idem, Nucl. Phys. B **695** (2004) 3.
12. A. Aktas *et al.* [H1 Collaboration], Eur. Phys. J. C **44** (2005) 1.
13. S. Chekanov *et al.* [ZEUS Collaboration], DESY-08-132, to be published in JHEP.
14. A. Aktas *et al.* [H1 Collaboration], Phys.Lett. B **659** (2008)796.
15. M. Derrick *et al.* [ZEUS Collaboration] Z. Phys. C **73** (1997) 253.
16. A. Freund, Phys. Rev. D **68** (2003) 096006.
17. E. Iancu, K. Itakura and S. Munier, Phys. Lett. B **590** (2004) 199.
18. K. Golec-Biernat and M. Wüsthoff, Phys. Rev. D **59** (1999) 014017.
19. A.M. Stašto, K. Golec-Biernat and J. Kwieciński, Phys. Rev. Lett. **86** (2001) 596.
20. A. Freund, K. Rummukainen, H. Weigert and A. Schäfer, Phys. Rev. Lett. **90** (2003) 222002.
21. C. Marquet and L. Schoeffel, Phys. Lett. B **639** (2006) 471.
22. M. Diehl, T. Gousset, B. Pire and J.P. Ralston Phys. Lett. B **411** (1997) 193.
23. A.V. Belitsky, D. Mueller and A. Kirchner, Nucl. Phys. B **629** (2002) 323.
24. H1 Collaboration, H1prelim-07-011, `http://www-h1.desy.de/h1/www/publications`.